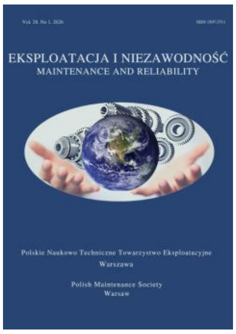

Eksploatacja i Niezawodnosc – Maintenance and Reliability
Volume 28 (2026), Issue 1
journal homepage: http://www.ein.org.pl

Article citation info:
Milewski M, Kierzkowski A, Kucharski M, Zielonka P, Inverse Method for Material Characterization of a UAV Composite Wing Based on FEM and Dynamic Response, Eksploatacja i Niezawodnosc – Maintenance and Reliability 2026: 28(1) http://doi.org/10.17531/ein/207312

Inverse Method for Material Characterization of a UAV Composite Wing Based on FEM and Dynamic Response

Indexed by: Web of Science Group

Maciej Milewski[a], Artur Kierzkowski[a,*], Mateusz Kucharski[a], Pawel Zielonka[a]

[a] Wrocław University of Science and Technology Faculty of Mechanical Engineering, Poland

Highlights

- Inverse identification method for composite materials based on dynamic response analysis.
- Integration of experimental and numerical modal analysis for material property estimation.
- Validated method applicable to UAV composite structures.
- Non-destructive approach enabling accurate FEM-based material calibration.

Abstract

This work introduces a method for the inverse identification of composite material properties using dynamic response data and finite element modelling. The methodology combines numerical modal analysis, Design of Experiments (DoE), Response Surface Methodology, and a Multi-Objective Genetic Algorithm (MOGA) to determine material parameters without destructive testing. The approach was applied to a UAV composite wing, achieving high correlation between simulated and experimental modal characteristics, with eigenfrequencies deviations below 2%. Variations between the identified parameters and reference data are linked to inherent inconsistencies in composite manufacturing and the operational condition of the tested structure. Nevertheless, the proposed method proves to be a reliable and non-invasive tool for estimating mechanical properties, enhancing the predictive capabilities of numerical models. Its adaptability makes it a promising solution for future applications in structural health monitoring, damage assessment, and optimization of aerospace composite structures.

Keywords
ground vibration test, composite structures, unmanned aerial vehicles, modal analysis, material characterization

1. Introduction

Since its inception, the aviation industry has continuously sought to minimize the weight of aerostructures to extend flight time, distance, and improve performance [1]. Modern composite materials have emerged as a revolutionary solution, offering an exceptional alternative to traditional metal structures. These materials provide an outstanding strength-to-weight ratio, excellent resistance to corrosion, and significant design flexibility, making them particularly well-suited for demanding aerospace applications. As a result, composites have found widespread use in manned aviation and the rapidly growing field of unmanned aerial vehicles (UAVs). In parallel with these developments, increasing environmental awareness has accelerated the search for sustainable alternatives to conventional composite systems. Natural fibre-reinforced polymers, bio-based resins, and recyclable composites are gaining traction across various sectors—including aerospace and UAV design—due to their reduced environmental footprint and favourable mechanical characteristics [2], [3], [4].

The unique characteristics of composites require tailored approaches to obtain their material properties. Traditional

(*) Corresponding author.
E-mail addresses: M. Milewski (ORCID: 0009-0005-6797-3151) maciej.milewski@pwr.edu.pl, A. Kierzkowski (ORCID: 0000-0003-2052-2167) artur.kierzkowski@pwr.edu.pl, M. Kucharski (ORCID: 0009-0008-6634-1568) m.kucharski@pwr.edu.pl, P. Zielonka (ORCID: 0000-0002-1178-3368) pawel.zielonka@pwr.edu.pl

strength tests, such as those assessing tensile and shear properties, are often time-consuming, costly, and require significant preparation. Consequently, there has been growing interest in alternative, indirect methods for determining material properties, particularly those that leverage structural responses under specific conditions. Indirect methods, such as inverse identification techniques, have shown significant promise by estimating material parameters, providing a more efficient alternative to direct testing [5].

Several methodologies have been proposed to address this challenge. Ragauskas and Belevičius [6] proposed a two – step methodology for identifying composite material properties, combining specimen geometry optimization with vibration testing. The authors focused on modifying specimen geometry to improve the identification of material properties, particularly Poisson's ratio, which is challenging to determine due to its low impact on eigenfrequencies. Rahmani et al. [7] developed an improved Regularized Model Updating (RMU) method for identifying composite material properties. This inverse technique addresses noise in displacement data, enhancing the Finite Element Model Updating (FEMU) approach using homogenization models as constraints, improving accuracy, especially for fibre properties. Kang et al. [8] proposed an inverse method using genetic algorithms (GAs) and finite element analysis to identify the mechanical properties of interfaces in multiphase composites. The method leverages experimental interfacial failure data as input for the identification process, enabling simultaneous estimation of tensile and shear properties in real microstructures under mixed-mode fracture. Chen et al. [9] introduced an innovative Approximate Bayesian Computation (ABC) framework to tackle the ill – posed inverse problem of identifying parameters in Variable Stiffness (VS) composite laminates. Lecompte et al. [10] identified an orthotropic composite's in – plane elastic parameters under biaxial loading using FEMU and full – field strain data. Geers et al. [11] applied an inverse identification method, using DIC data, to determine the parameters of a gradient-enhanced damage model for glass-fibre-reinforced polypropylene composites. Liu et al. [12] employed an inverse identification method to determine the nonlinear mechanical properties of carbon fibre-reinforced composites under dynamic loading, obtaining strain- and frequency-dependent expressions for elastic moduli and loss factors through experimental testing and inverse analysis, validated by numerical models. Karpenko et al. [13] applied an inverse approach, combining theoretical and experimental methods, to analyse the dynamic properties of composite pneumatic tyres, using piezoelectric micro-vibration tests and FEM simulations, with high accuracy between experimental and numerical results. Lopes et al. [14] present a modelling-based approach to predict cork-rubber composites' static and dynamic performance, applying inverse methods through linear regression and finite element analysis (FEA).

While inverse methods have been extensively used for parameter identification, their integration with vibrational data provides additional information about material properties and structural performance. Not only does it provide valuable insights into the material constants, but it also delivers critical information about structural health and the operational state of the object. This makes vibrational data particularly powerful for detecting degradation, identifying damage, and understanding how external conditions—such as varying loads or environmental factors—influence the structure's performance. For example, Wittig et al. [15] proposed a vibration-based ice monitoring method for composite blades using artificial neural networks under different icing conditions. In Ooijevaar et al. [16] study vibration-based damage identification method using the Modal Strain Energy Damage Index successfully detected and localized delamination in a carbon fibre PEKK T-beam. Liang et al. [17] conducted a study focusing on predicting the residual fatigue life of fibre-reinforced polymer (FRP) structures using vibration parameters.

While the unique properties of composites have revolutionized the aerospace industry, their complex characterization remains a persistent challenge. Current research often focuses on simplified geometries. Tam et al. conducted a study on the identification of material properties of composite plates using Fourier-generated frequency response functions on a model of a simple orthotropic plate [18]. Teixeira Silva et al. conducted a study aiming to present a technique for identifying the elastic parameters of composite materials. The proposed technique was validated through various tests, applied to plates made from different materials, ranging from isotropic to orthotropic [19]. Hwang et al. proposed a numerical method that combines finite element analysis with a hybrid genetic algorithm to inversely identify the elastic constants of composite materials based on vibration testing data. They performed experimental tests on rectangular plates with different thickness and stacking sequences [20]. Araujo et al. proposed a combined numerical–experimental method aimed at identifying six elastic material moduli of generally thick composite plates. Their technique is versatile and applicable to composite plates made from various materials and with arbitrary stacking sequences [21]. Sankar et al. presented an innovative approach for identifying material properties of composite plates using a hybrid method that combines Response Surface Methodology (RSM) with Particle Swarm Optimization (PSO). Initially, various RSM and PSO strategies were evaluated using a simplified 4 degrees-of-freedom (4DOF) dynamic system to assess their speed and accuracy [22]. Ismail et al. proposed a methodology for determining the material properties of orthotropic plates with general elastic boundary conditions using an inverse approach. In this method, the identification of material properties was achieved by updating four parameters within the governing equation for a symmetrically laminated thin plate [23]. This study seeks to address this gap by applying inverse identification methods based on Ground Vibration Test (GVT) and FEM analysis to determine the material properties of UAV composite wing structures. By integrating experimental data with computational models in Ansys software, the approach aims to validate simulation techniques for more intricate configurations, extending their applicability beyond basic specimens. By addressing geometry and computational modelling challenges, it seeks to optimise composite materials for demanding aerospace applications, demonstrating the potential of inverse methodologies.

Modal analysis (or Ground Vibration Test) is a widely employed non-destructive testing (NDT) method, valued for its ability to assess structures' integrity and dynamic behaviour without compromising their functionality. This makes it particularly suitable for applications in aerospace engineering, where destructive testing is often impractical due to the critical nature and high cost of components. Moreover, extracting material samples for direct testing often renders components unusable for composite materials, highlighting the practical importance of non-destructive methods like GVT. This approach allows engineers to maintain the operational state of the structure while gaining valuable insights for further computational modelling and optimization.

By preserving the structural integrity of key elements, such as UAV wings or fuselage sections, GVT provides plenty of information about the system's properties. These include not only its dynamic characteristics, such as eigenfrequencies, mode shapes, and damping ratios but also its overall structural health. For example, changes concerning the reference vibration parameters can indicate the presence of damage, material degradation, or changes in boundary conditions, making GVT a powerful diagnostic tool in structural health monitoring (SHM) [24], [25], [26].

In practice, different types of modal analysis may be employed. For instance, GVT is performed under controlled laboratory conditions—often under free–free or simply supported boundary conditions—to capture the natural vibrations of the structure [27] [28]. Operational modal analysis (OMA), on the other hand, involves analysing the dynamic response of a structure under its actual operational conditions without imposing artificial excitation [29] [30].

Data acquisition during modal testing is typically carried out using a network of accelerometers or laser vibrometers, which record structure’s response at multiple discrete points. The coherence between measurement channels is essential to ensure the reliability of the captured mode shapes and eigenfrequencies. In modal analysis, coherence is a key metric used to evaluate the quality and reliability of measured data [31]. It describes how much the structural response correlates with the applied excitation force across the frequency spectrum. Maintaining high coherence is crucial for extracting reliable modal parameters. A well-positioned excitation force typically applied using an electrodynamic shaker or impact hammer, should generate a response strongly correlated with the input, leading to coherence values near 1 across the frequency range of interest [32].

Fundamental equation of dynamic behaviour of a structure can be described as:

$$[\boldsymbol{M}]\{\ddot{x}\} + [\boldsymbol{C}]\{\dot{x}\} + [\boldsymbol{K}]\{x\} = \{f\}, \tag{1}$$

where $[\mathbf{M}]$, $[\mathbf{C}]$ and $[\mathbf{K}]$ are global mass, damping and stiffness matrices respectively, and $\{\ddot{x}\}$ is acceleration vector, $\{\dot{x}\}$ is velocity vector and $\{\mathrm{x}\}$ is displacement vector of dynamic system; {f} is excited force vector.

If external load and damping effects are not considered, the equation becomes:

$$[\boldsymbol{M}]\{\ddot{x}\} + [\boldsymbol{K}]\{x\} = 0, \tag{2}$$

then replace the characteristic equation of $\{x\}$ by the solution of $\phi_i sin\omega_i t$ Eq. (2) is transferred to:

$$([\boldsymbol{K}] - \omega_i{}^2[\boldsymbol{M}])\{\phi_i\} = 0, \tag{3}$$

where $\{\phi_i\}$ is mode shape of ith eigenfrequency and ω_i is ith eigenfrequency of the structure.

Unlike isotropic materials, where stiffness is uniform in all directions, composites exhibit direction – dependent behaviour due to their layered constructions. Factors such as fibre orientation, ply thickness, stacking sequences, and percentage of fibres in a composite play a crucial role in defining the stiffness characteristics of the structure.

To accurately capture this complexity, Classical Laminate Theory (CLT) is often employed to construct the stiffness matrix for composite materials [33]. CLT models the laminate as a stack of orthotropic plies, each contributing to the overall stiffness matrix. Stack of plies is shown in Figure 1.

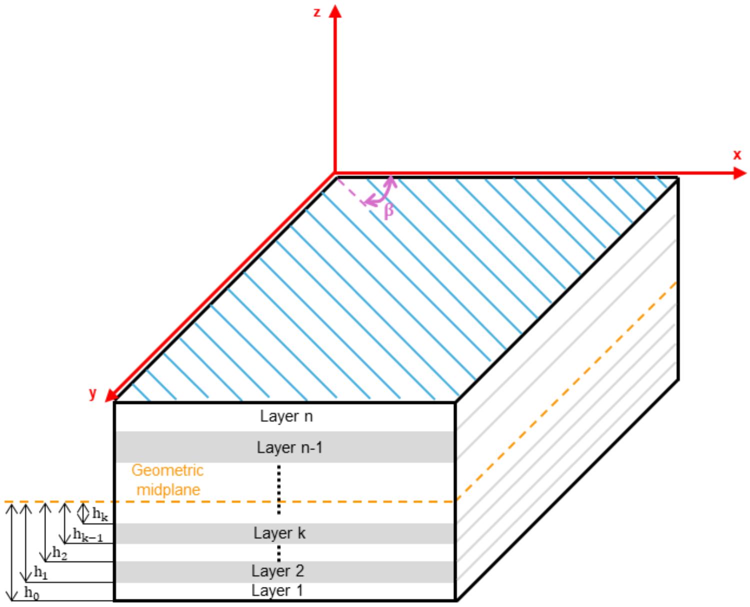

Figure 1. Scheme of the stack of plies.

The stiffness matrix for laminate can be expressed as:

$$\boldsymbol{K} = \begin{bmatrix} A_{11} & A_{12} & A_{16} & B_{11} & B_{12} & B_{16} \\ A_{12} & A_{22} & A_{26} & B_{12} & B_{22} & B_{26} \\ A_{16} & A_{26} & A_{66} & B_{16} & B_{26} & B_{66} \\ B_{11} & B_{12} & B_{16} & D_{11} & D_{12} & D_{16} \\ B_{12} & B_{22} & B_{26} & D_{12} & D_{22} & D_{26} \\ B_{16} & B_{26} & B_{66} & D_{16} & D_{26} & D_{66} \end{bmatrix}, \tag{4}$$

where A_{ij}, B_{ij} and D_{ij} are the extension, coupling and bending stiffness matrices, respectively, defined as:

$$A_{ij} = \sum_{k=1}^{N} \overline{Q_{ij}}^k (h_k - h_{k-1}), B_{ij} = \frac{1}{2}\sum_{k=1}^{N} \overline{Q_{ij}}^k ({h^2}_k - {h^2}_{k-1}), D_{ij} = \frac{1}{3}\sum_{k=1}^{N} \overline{Q_{ij}}^k ({h^3}_k - {h^3}_{k-1}), \tag{5}$$

where N is the number of layers of the composite, h_k represents the distance from the middle plane to the upper and lower surface. The transformed stiffness matrix $\overline{\boldsymbol{Q}}^k$ can be defined as:

$$\overline{\boldsymbol{Q}}^k = \boldsymbol{T} \cdot \boldsymbol{Q} \cdot (\boldsymbol{T}^{-1})^T, \tag{6}$$

where $\boldsymbol{T}$ is the matrix for transformation from the global coordinate system to the principal coordinate system, defined as:

$$\boldsymbol{T} = \begin{bmatrix} cos^2\beta & \sin^2\beta & 2sin\beta cos\beta \\ \sin^2\beta & cos^2\beta & -2sin\beta cos\beta \\ -sin\beta cos\beta & sin\beta cos\beta & cos^2\beta - \sin^2\beta \end{bmatrix}, \tag{7}$$

where β is the angle between the two coordinate directions. The stiffness matrix $\boldsymbol{Q}$ for single lamina, in the principal coordinate system can be expressed as:

$$\boldsymbol{Q} = \begin{bmatrix} Q_{11} & Q_{12} & 0 \\ Q_{21} & Q_{22} & 0 \\ 0 & 0 & Q_{66} \end{bmatrix}, \tag{8}$$

where

$$Q_{11} = \frac{E_{11}}{1-\upsilon_{12}\upsilon_{21}}, Q_{12} = Q_{21} = \frac{\upsilon_{12}E_{22}}{1-\upsilon_{12}\upsilon_{21}}, Q_{22} = \frac{E_{22}}{1-\upsilon_{12}\upsilon_{21}}, Q_{66} = G_{12}, \tag{9}$$

where E_{11} and E_{22} are the elastic moduli, G_{12} is the shear modulus, and υ_{12} and υ_{21} are the Poisson's ratios.

Only four out of the five material constant for plane stress of an orthotropic material are independent. The Poisson's ratio υ_{21} is obtained as:

$$\upsilon_{21} = \frac{\upsilon_{12}E_{22}}{E_{11}}. \tag{10}$$

Given that Young's moduli and other elastic properties govern the stiffness matrix of composite materials, their precise identification is essential for accurate structural modelling. The strong dependency of dynamic behaviour on these parameters highlights the necessity of high fidelity identification techniques.

2. Materials and Methods

In this study, we propose an inverse identification method that leverages GVT data to determine composite wing structures' material properties accurately. The method refines the numerical model by adjusting key parameters – such as Young's moduli, shear modulus– until the simulated dynamic response aligns with the experimental measurements. This approach provides a robust, non-destructive alternative to conventional testing methods.

The method flow is presented in Figure 2. The key methodical steps requiring further elaboration are detailed in the following sections. Section 2 explores part A of method with the fundamentals of modal analysis and Classical Laminate Theory (CLT) in the context of composite materials and outlines the B part of method, including the application of Response Surface Methodology (RSM) and Design of Experiment (DoE) within Ansys. Section 3 presents the practical implementation and validation of the proposed approach.

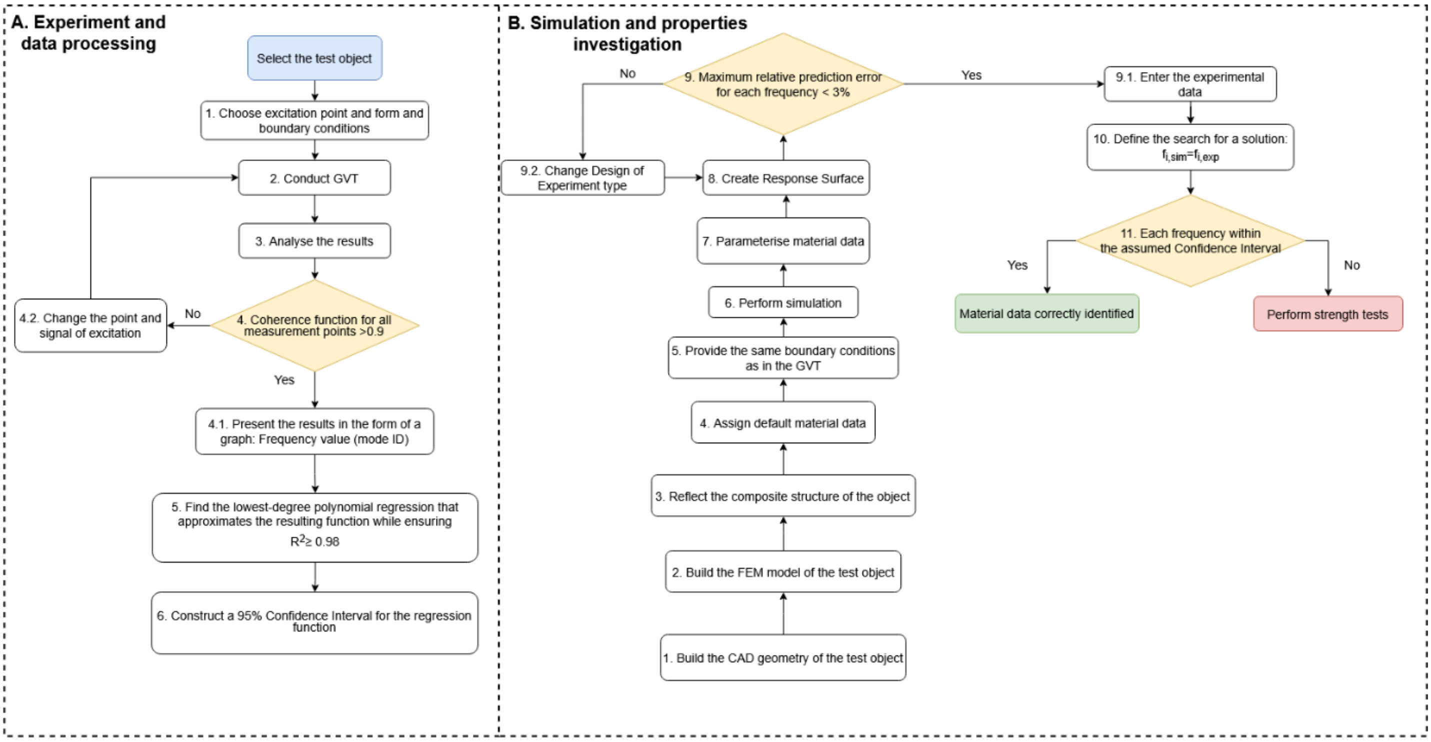

Figure 2. Investigation procedure flowchart.

2.1. Ground Vibration Test

The identification process begins with selecting the test object, followed by the definition of boundary conditions and excitation points. A GVT is performed to extract the Frequency Response Function (FRF), from which modal parameters such as eigenfrequencies and mode shapes are derived. To ensure high measurement quality, the coherence function is analyzed. If coherence is low, modifications to the excitation points or levels may be necessary to improve data quality. The obtained eigenfrequencies are further processed by fitting a polynomial regression function of the lowest possible degree while ensuring a coefficient of determination $R^2 \geq 0.98$. The value of R^2 should be greater than 0.7 for a good fitting quality [34]. Based on this function, a 95% confidence interval is constructed, which will later serve as a criterion for evaluating the accuracy of the numerical results. Both criteria were adopted as a best practice in statistical analysis to ensure the reliability and accuracy of the results. A coefficient of determination of at least 0.98 indicates an excellent fit of the regression model to the data, minimizing the discrepancy between predicted and observed values. Meanwhile, the 95% confidence interval is typical value applied in engineering data [35]. These thresholds were chosen to guarantee high precision in the optimization process while maintaining statistical rigor.

2.2. Numerical Model

The essential step in the identification process is representing the test object using a CAD environment and conducting a numerical modal analysis. The accuracy of the simulation depends on correctly defining boundary conditions and mesh discretization. Commonly applied boundary conditions include free-free, clamped or simply supported configurations, chosen based on experimental constraints to ensure consistency between numerical and operational conditions. At this stage, default material data is introduced, typically derived from literature values, software library or manufacturer specifications. These initial properties serve as a baseline and will be systematically refined throughout the identification process.

2.3. Design of Experiment and Response Surface Methodology

A Design of Experiments approach is employed to explore the relationship between material properties and dynamic response efficiently. DoE provides a structured methodology for selecting representative material parameter sets, reducing computational costs compared to exhaustive simulations. Several DoE techniques can be applied, depending on the complexity of the problem. Full-factorial design**s** evaluate all possible parameter combinations but quickly become impractical in high-dimensional problems [36]. Latin Hypercube Sampling (LHS) ensures uniform coverage of the design space and is widely used in engineering optimization [37]. A more efficient alternative is Sparse Grid Sampling (SGS), strategically placing sample points toa balance computational efficiency and accuracy. This method is particularly advantageous in high-dimensional parameter spaces, where a reduced number of simulations is desirable without compromising predictive capabilities [38].

Once an appropriate DoE strategy is selected, a process is conducted for each sampled material configuration. These simulations generate a dataset that describes how variations in material properties affect eigenfrequencies. Instead of directly optimizing material parameters using finite element simulations—which would be computationally expensive—a Response Surface Methodology is employed to construct a surrogate model. RSM approximates the relationship between material properties and modal characteristics, significantly reducing computational demands by allowing rapid interpolation of modal parameters within the explored design space.

Once an appropriate DoE strategy is selected, simulations are performed for each sampled material configuration, generating a dataset that characterizes the influence of material properties on eigenfrequencies. Instead of directly optimizing material parameters through computationally expensive finite element simulations, RSM is employed to construct a surrogate model. RSM approximates the relationship between material properties and modal characteristics, significantly reducing computational costs by enabling rapid interpolation of modal parameters within the explored design space.

2.4. Model Evaluation and Optimization

The next step involves evaluating the accuracy of the surrogate model. The simulated eigenfrequencies are compared against the experimental confidence intervals. If the maximum relative prediction error for each frequency remains below 3%, the chosen DoE type is validated, and the simulation data can be further used in the optimization process. However, if the discrepancies exceed this threshold, the DoE approach must be adjusted to improve model accuracy.

Once a reliable response surface is established, the experimental frequencies are introduced into the solver, which searches for material parameters that satisfy the condition $f_{i,sim} = f_{i,exp}$. This optimization process refines the material properties iteratively to minimize deviations between experimental and simulated modal characteristics. After obtaining optimized parameters, the final verification step checks whether the resulting frequencies fall within the predefined confidence interval. If all values are within the assumed range, the material identification is considered successful. However, if discrepancies persist, material tests are required to perform.

By integrating numerical modal analysis, DoE, response surface modelling, and optimization, this method provides a systematic framework for identifying material properties while minimizing computational costs and avoiding destructive testing. The iterative approach ensures high precision in material characterization, making it a valuable tool for applications in structural health monitoring, damage detection, and lifespan estimation of composite structures.

3. Practical Application

This section presents the application of the proposed inverse identification method to determine the material properties of a composite structure used to manufacture UAV wing. Wing is presented in Figure 3.

Figure 3. Test object.

Previous work [39] provides a detailed description of the experimental and numerical modal analysis. To exclude external constraints, the experimental modal analysis was conducted on a carbon-epoxy UAV wing structure under free boundary conditions. The structure was excited using an electrodynamic shaker, and the response was measured at 27 discrete points using high-sensitivity accelerometers. The recorded acceleration signals were processed to extract eigenfrequencies and mode shapes, which served as reference data for subsequent numerical modelling.

3.1. Initial numerical model

A finite element model of the wing was developed using Ansys ACP, where the laminate stacking sequence, including layer orientations, thicknesses, and material assignment, was explicitly defined. The detailed stacking sequence is illustrated in Figure 4, and carbon-fibre layer directionality is illustrated in Figure 5.

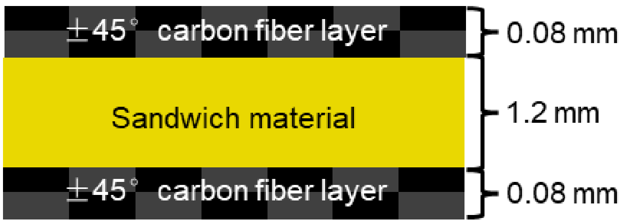

Figure 4. Stacking sequence of each half.

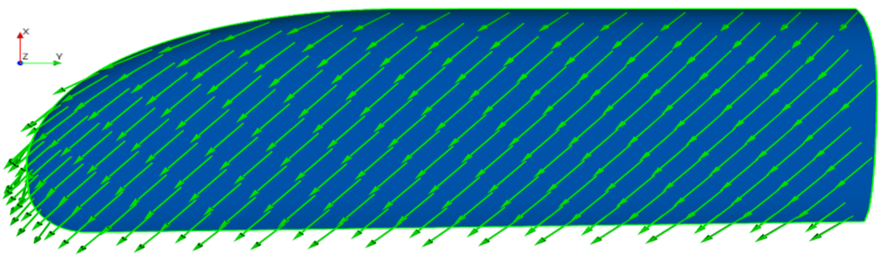

Figure 5. Direction of carbon fibre assigned in ACP module.

To represent the experimental conditions, the simulation was conducted under free-free boundary conditions, and the modal analysis was performed to extract eigenfrequencies and mode shapes.

At this stage, default material properties were used, selected from the software's material database (Epoxy Carbon Woven (230 GPa) Wet). Table 1 presents the material properties.

Table 1. Default material properties.

Property	Value
Density	1.79 g/cm^3
E_x	59.61 GPa
E_y	59.61 GPa
G_{xy}	3.3 GPa
v_{xy}	0.04

The comparison of baseline numerical results with experimental modal data (Table 2) revealed discrepancies in eigenfrequencies, necessitating further refinement of the material parameters. The difference was calculated using the experimental result as the reference value. The percentage difference shown in the table was calculated using the formula:

$$Difference = \left|\frac{Simulation - Experiment}{Experiment}\right| * 100\% \quad (11)$$

Table 2. Comparison of numerical and experiment results [39].

Mode ID	Simulation [Hz]	Experiment [Hz]	Experiment value range [Hz]	Difference [%]
1	86.35	79.85	<79.4;80.02>	8.18
2	125.58	114.94	<113.81;115.08>	9.26
3	139.89	134.98	<134.4;135.82>	3.64
4	162.03	157.75	<157.02.4;158.642>	2.71

For the results obtained, the frequency – mode ID relationship was approximated by a linear function, as this turned out to be the lowest degree polynomial giving an R^2 greater than 0.98. The function and the 95% confidence intervals constructed for it are shown in Figure 6.

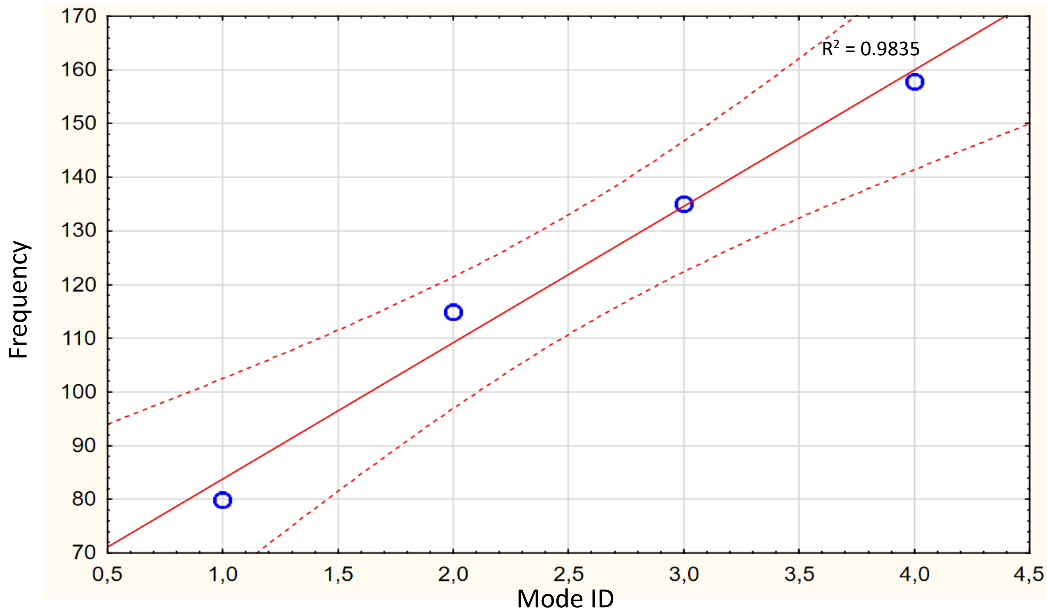

Figure 6. Regression function and Confidential Interval for obtained results. Blue circles - results from the experiment. Red solid line - regression function. Red dashed line - confidence interval limits

3.2. Optimization Process

Despite the satisfactory correlation between the experimental and simulated mode shapes, a more precise identification of the material properties is required. This is essential for improving the accuracy of future numerical analyses, particularly for predicting structural responses under varying operational conditions. A refined material model enables a better assessment of the aircraft's structural integrity, supporting decisions related to continued operation, potential modifications, and life-extension strategies. The observed discrepancies indicate that the default material properties do not accurately represent the UAV wing composite. The next step involves optimising these material parameters, following the method outlined in the flowchart. The applied bounds for the optimization were as follows:

$$\begin{cases} 25\ GPa \le E_x, E_y \le 85\ GPa \\ 1\ GPa \le G_{xy} \le 10\ GPa \end{cases},$$

where x corresponds to the fibre direction and y is transverse direction.

By constraining the search space within these ranges, the optimization was prevented from converging to non-physical solutions, ensuring that the identified material parameters were representative of the actual composite structures used in the UAV wings. The selected constraints were based on the dataset presented in [40], which provides a comprehensive collection of experimentally obtained material properties for various composite specimens. This database includes mechanical characteristics of composites manufactured using similar fabrication techniques, reinforcing the validity of the assumed parameter bounds. By leveraging this empirical foundation, the optimization process remained grounded in realistic material behaviour, improving the reliability of the identified properties and their applicability to real-world aerospace structures. The Poisson's ratio was not included in the identification process, as its influence on the resulting eigenfrequencies was found to be negligible [6].

Since the carbon fibre material used in the UAV wing is woven, the same material properties were assumed for both the E_x and E_y directions. This is because woven carbon fibre exhibits quasi-isotropic behaviour in-plane, meaning that its stiffness is identical in both fibre and transverse directions.

It is important to note that the core material of the sandwich composite structure is isotropic and typically provided with well-documented material properties by the manufacturer [41]. As a result, it does not require parameterization since its exact characteristics are known and remain constant throughout the analysis. This allows us to focus solely on the identification of the carbon-fibre laminate properties.

To efficiently explore the relationship between material properties and eigenfrequencies, Sparse Grid Sampling was chosen as the DoE method due to its effectiveness in handling nonlinear problems while maintaining a balance between accuracy and computational efficiency. The optimization process utilized 111 sample points, yielding a maximum relative prediction error for the first four eigenfrequencies: mode 1: 2.05%, mode 2: 2.34%, mode 3: 2.89%, mode 4: 2.74%. The generated Response Surface illustrating the relationship between Young's modulus, shear modulus and the mode 1 value is presented in the Figure 7.

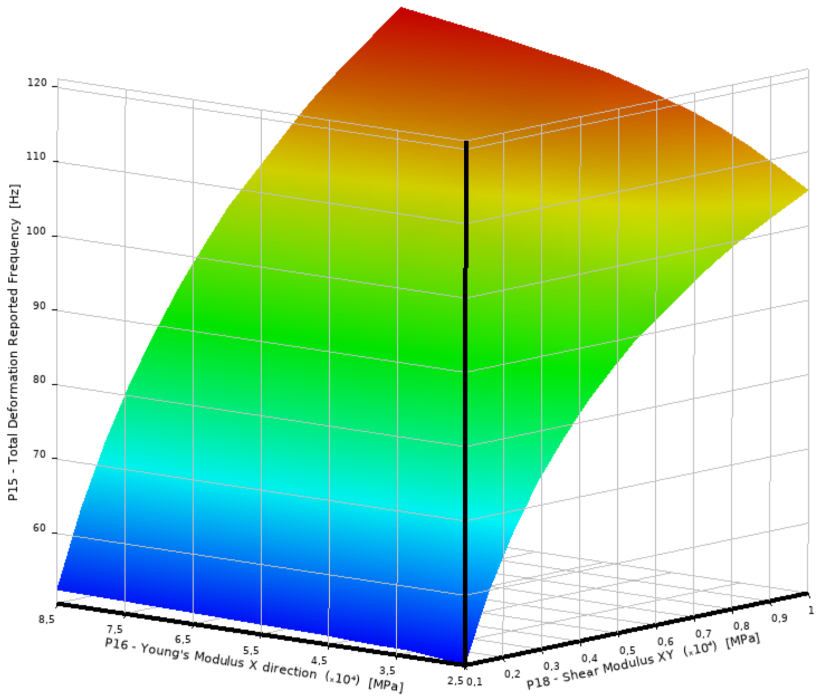

Figure 7. Response Surface relationship between $\boldsymbol{E_x}$, $\boldsymbol{G_{xy}}$, and mode.

Since all error values remained below the 3% threshold, the response surface model was deemed sufficiently accurate, and the optimization process proceeded. The next step involved refining the material parameters using the validated surrogate model to ensure minimal deviation between the experimental and simulated modal characteristics.

The optimization process was carried out using the Multi-Objective Genetic Algorithm (MOGA), an advanced variant of NSGA-II (Non-dominated Sorted Genetic Algorithm-II), employs controlled elitism to balance exploration and exploitation of the search space, making it well-suited for complex, multi-objective problems [42]. MOGA is specifically designed to handle multi-objective optimization problems by simultaneously optimizing multiple conflicting objectives while maintaining a diverse set of solutions. This is achieved through the application of controlled elitism, which ensures a balance between exploration and exploitation of the search space, preventing premature convergence to local optima and enhancing the robustness of the solution. In multi-objective optimization problem can be described as [43]:

$$Minimize\ F(p) = [F_1(p), F_2(p), \dots, F_M(p)],$$

where $p \in \Re^d$, subject to $g_j(p) \leq 0, j = 1, 2, \dots, J; h_k(p) = 0, k = 1, 2, \dots, K,$

where p represents the vector of design variables, $F(p)$ denotes the vector of objective functions, and g_j and h_k define inequality and equality constraints, respectively. The space $\mathcal{F} = \Re^d$ spanned by the vectors of design variables p is called the search space. The space $S = \Re^M$ formed by all the possible values of objective functions is called the solution space.

In contrast to single-objective optimization, multi-objective optimization does not always yield a single solution that minimizes all objective functions simultaneously. This is because objectives often conflict with one another, meaning that improving one objective may come at the cost of worsening another. As a result, the optimal parameters for one objective may not necessarily lead to the best outcomes for the others, and in some cases, they may even have a negative impact.

Originally developed by Deb et al. [44], NSGA-II has gained significant popularity in solving multi-objective optimization problems due to its ability to identify multiple Pareto-optimal solutions. Its key features include elitist selection mechanisms, diversity preservation, and a strong emphasis on maintaining a set of non-dominated solutions throughout the optimization process.

Unlike single-objective optimization, where a unique global optimum is sought, multi-objective optimization involves conflicting objectives, meaning that improving one criterion may lead to the deterioration of another. As a result, rather than a single optimal solution, the outcome is a Pareto front-a set of non-dominated solutions where no single solution is strictly better than another across all objectives.

In NSGA-II, the optimization process begins by generating an initial population, from which offspring are created through standard genetic operators such as crossover and mutation. The new population is then merged with the parent population, forming a combined set of solutions. A non-dominated sorting procedure is applied to rank the solutions into Pareto fronts, where the first front consists of solutions that are not dominated by any other, the second front consists of solutions dominated only by those in the first front, and so on. To maintain the population size, solutions are selected iteratively from the sorted fronts until the required number is reached. If a front exceeds the remaining capacity, a crowding distance metric is used to prioritize solutions with higher diversity, ensuring an even distribution across the Pareto front.

The crowding distance plays a crucial role in maintaining solution diversity. It is calculated based on the relative spacing of solutions within the objective space, ensuring that selected solutions are well-distributed rather than clustered in specific regions. During the selection process, solutions are compared based on their rank, with higher-ranked solutions preferred. If two solutions share the same rank, the one with a greater crowding distance is chosen, thereby promoting diversity.

The iterative nature of NSGA-II ensures that the population evolves toward an improved Pareto front over successive generations.

In this case, MOGA iteratively refined the key material parameters within the predefined constraints to minimize the objective function $F(p)$, ensuring close agreement between the simulated and experimental data. Its ability to navigate non-linear dependencies and multimodal optimization landscapes allowed for an efficient convergence toward an optimal material parameter set, improving the accuracy of the numerical model.

The objective function, $F(p)$, quantifies the discrepancy between experimental and simulated eigenfrequencies:

$$F(p) = \left(\frac{|f_{i,exp} - f_{i,sim}|}{f_{i,exp}}\right) \cdot 100\%, \tag{12}$$

where $f_{i,exp}$ and $f_{i,sim}$ are the ith experimental and simulated eigenfrequencies, respectively and p is the vector of unknown material properties.

Table 3 presents a comparison of frequency obtained from experiment and optimized simulation.

Table 3. Comparison of experiment and optimized simulation results.

Mode ID	Experiment [Hz]	Optimized simulation [Hz]	$F(p)$ [%]
1	79.85	80.99	1.43
2	114.94	112.82	1.84
3	134.98	135.21	0.16
4	157.75	155.63	1.34

3.3. Mechanical tests of material samples

After optimization, the discrepancies between the numerical and experimental results were reduced below 2% for all analysed modes, with the highest error observed at Mode 2 (1.84%). For the optimized frequency values, the algorithm provided the corresponding optimized material properties: E_x, E_y = 47126 MPa , G_{xy} = 3927 MPa . To assess the accuracy and effectiveness of the proposed method, physical material testing was conducted. The specimens were prepared and subjected to the following mechanical testing to determine the in-plane elastic properties:

- Static tensile tests in accordance with ASTM D3039 [45]
- Static compression tests following ASTM D6641 [46]
- Static shear tests based on ASTM D7078 [47]

These experimental results provided a direct comparison with the computationally identified material parameters, serving as a validation of the inverse identification approach. The specimens were manufactured using the same fabrication method as the UAV wing – hand lay-up with vacuum bagging. From the resulting composite laminate, test samples were cut to the dimensions specified in the previously referenced ASTM standards. This ensured consistency between the material properties of the tested specimens and those of the actual structure, allowing for a reliable validation of the identified parameters. Specimens prepared for mechanical testing are shown in the Figure .

a)

b)

c)

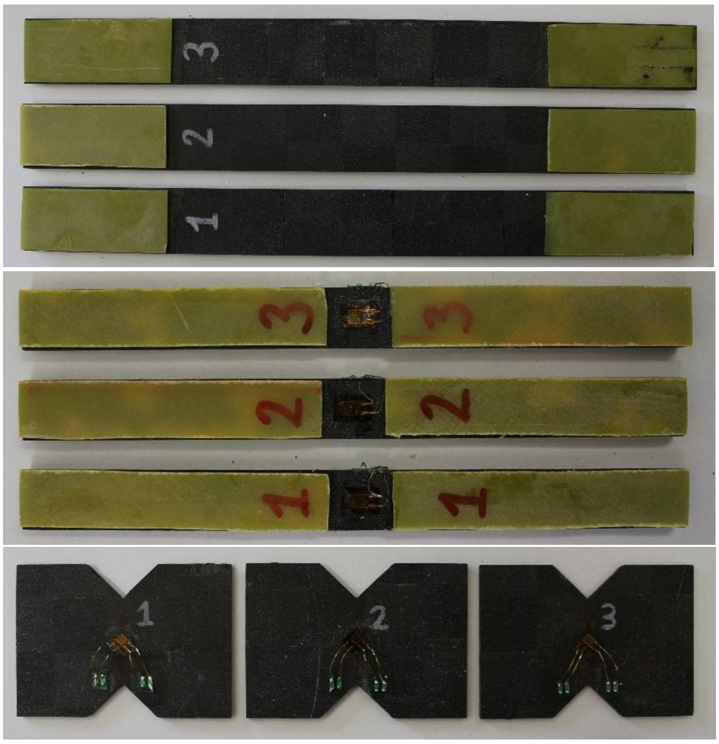

Figure 8. Specimen prepared for mechanical testing a) tensile tests, b) compression tests, c)shear tests.

For each type of the test 3 specimens were performed with experimental parameters presented in

. The elastic properties of composite materials were obtained using data collected from testing machine and strain gauges. For static tensile tests the extensometer were used, which measure elongation of the specimen until 0.5% value. For compression and shear tests, the strain gauges were sticked by cyanoacrylate glue and connected into quarter bridge with an external dummy strain gauge.

Table 4. Experimental parameters.

Type of tests	Testing machine	Velocity	Strain measurement
Static tensile tests	Instron 5982 with 100kN loading cell	2mm/min	2630-100 series extensometer with 50 mm gauge length
Static compression tests	MTS 858 with 15kN loading cell	1.2mm/min	Strain gauge TF-3/120 with 3mm base
Static shear tests	MTS 810 with 250kN loading cell	1.2mm/min	Strain gauge TFs-3-2x/120 with 3mm base

Table 5. Obtained mechanical properties from experimental campaign.

Property	**Mechanical Tests [MPa]**	**Simulation [MPa]**	**[%]**
E_x, E_y (from tensile)	43181	47126	9.14
E_x, E_y(from compression)	53588		12.1
E_x, E_y(mean value)	48385		2.6
G_{xy}(0.15-0.55%)	3650	3927	7.58
G_{xy}(0.15-0.35%)	3973		1.16
G_{xy}(0.15-0.25%)	4163		5.67
G_{xy}(0-0.40%)	4232		7.21

Comparison of the mechanical properties taken from experimental campaign and simulation studies are shown at Table 5. The variation of obtained results was achieved dividing values taken from simulation by properties from mechanical test.

The percentage differences presented in Table 5 were calculated according to the formula:

$$Difference = \left|\frac{Simulation - Mechanical\ Test}{Mechanical\ Test}\right| * 100\% \qquad (13)$$

The stiffness along to fibre axis acquire from compression and tensile test is characterized by fairly large difference in value. In both cases, the outcome from simulation is characterize with discrepancy from experimental data. If the mean value calculated from the tensile and compression results will be compared with simulation, the convergence can be observed. This phenomenon can be noticed cause wing under bending have one side of the structure working in tensile regime, when second side is compressed. Comparing shear properties is more challenging, due to non-linear properties of the laminate under shear stress. The value of (13) nly depends on the range of shear strain used for desig elastic property. The ASTM standard recommend calculation of the shear modulus of elasticity applied over a 0.4% of engineering shear strain range and starting with lower strain point from 0.15% to 0.25%. Variation of obtained shear modulus in different strain range were presented on Table 5. Obtained mechanical properties from experimental campaignTable and

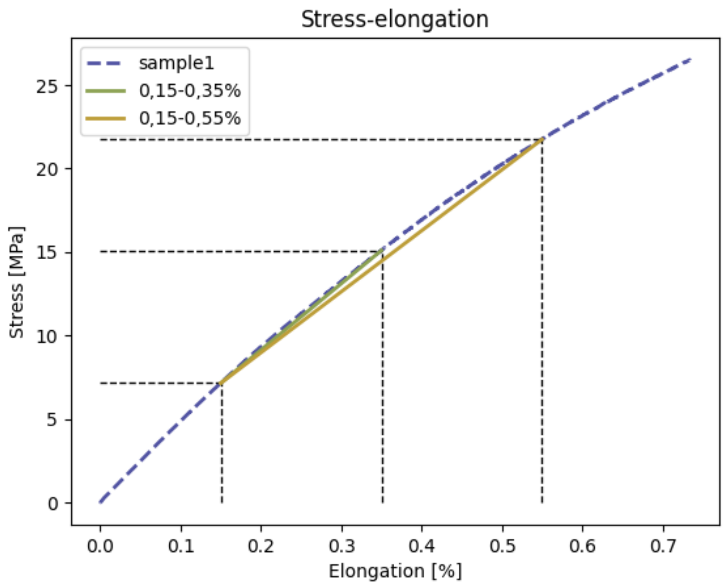

Figure 9. Result of stress-elongation plot obtain from shear test.

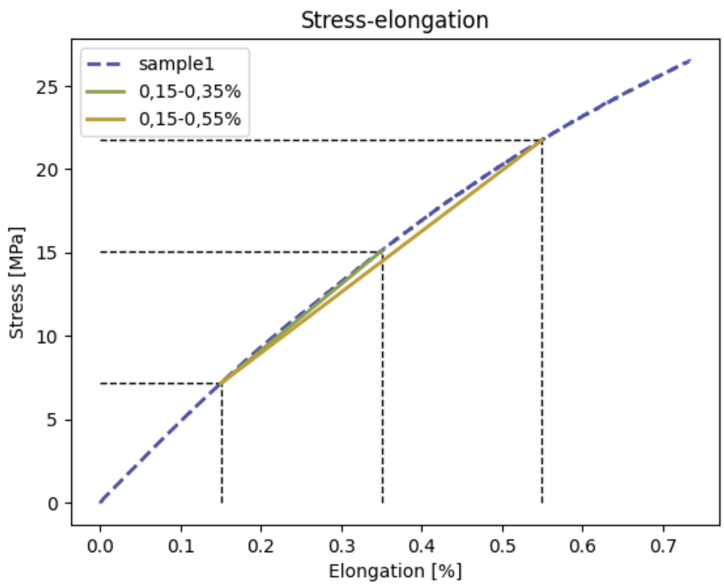

Figure 9. Result of stress-elongation plot obtain from shear test.

However, despite maintaining the same manufacturing process and materials, there is no absolute certainty that the fibre volume fraction in the composite is identical across all specimens. Since the fabrication process involves hand lay-up and vacuum bagging, slight variations in resin content and fibre distribution may occur. These inconsistencies can lead to minor differences in mechanical properties between the test samples and the structural component, potentially influencing the correlation between experimental and simulated results.

Subsequently, the experimentally determined material properties were incorporated into the simulation model, and a modal analysis was conducted using these parameters. This step aimed to evaluate how well the experimentally obtained constants reproduce the dynamic behaviour of the structure in the numerical model. Table 6 presents a comprehensive comparison of eigenfrequencies obtained from the experiment, the initial simulation, the optimized simulation, and the simulation based on the material properties derived from mechanical testing.

Table 6. Eigenfrequency Comparison: Experiment vs. Simulations.

Mode ID	GVT [Hz]	Init. Sim. [Hz]	Difference vs GVT [%]	Opt. Sim. [Hz]	Difference vs GVT [%]	Sim. (Exp. Mat.) [Hz]	Difference vs GVT [%]
1	79.85	86.35	8.18	80.99	1.43	78.47	1.72
2	114.94	125.58	9.26	112.82	1.84	111.93	2.61
3	134.98	139.89	3.64	135.21	0.16	133.06	1.42
4	157.75	162.03	2.71	155.63	1.34	156.86	0.56

4. Conclusion

The study presents a validated methodology for inverse identification of composite material properties using dynamic testing and numerical modelling. The proposed approach, integrating DoE, RSM, and MOGA, was successfully applied to a UAV wing structure demonstrating its capability to refine material properties and improve the accuracy of numerical simulations.

The optimization process led to a significant reduction in relative error across all considered modes. As shown in Table 3, the maximum discrepancy between the optimized simulation and experimental frequencies did not exceed 1.84%, indicating very high consistency between the model and the actual structural response. Notably, the largest improvement was observed in Mode 2, where the error was reduced from over 9% (initial simulation) to below 2% after optimization.

This improvement reflects the effectiveness of the adopted algorithm in handling non-linear dependencies between material constants and dynamic response. The inverse identification yielded optimized values of E_x, E_y = 47126 MPa , G_{xy} = 3927 MPa, which were further validated against mechanical testing results.

Experimental tests conducted on specimens manufactured using the same technique as the UAV wing (hand lay-up with vacuum bagging) revealed some variation in measured stiffness values. Tensile and compression tests showed a considerable spread in E_x, E_y (43181 MPa vs. 53588 MPa), primarily due to differences in loading regime and local imperfections. However, when the mean value (48385 MPa) was considered, the difference with respect to the optimized simulation was reduced to 2.6%, confirming the method's reliability.

Shear modulus G_{xy} showed higher variability, depending strongly on the selected shear strain range. This is expected due to the non-linear behaviour of composite laminates in shear. As presented in Table 5 and Figure 9, different shear ranges (e.g., 0.15–0.25%, 0.15–0.35%) produced moduli ranging from 3650 MPa to 4232 MPa. The optimized value (3927 MPa) falls within this range and aligns most closely with the modulus obtained for the ASTM-recommended range (0.15–0.35%), differing by only 1.16%. This supports the accuracy of the inverse method, while also highlighting the need for careful selection of strain range when determining shear properties experimentally.

The optimization process significantly reduced initial discrepancies between simulated and experimental frequencies, with final deviations remaining below 2% for all analysed modes. However, while the numerical model was improved, certain limitations and challenges must be acknowledged.

A key aspect influencing the accuracy of the identified material properties is the variation in composite manufacturing conditions. Differences in fibre volume fraction, resin content, and potential imperfections inherent in hand lay-up vacuum bagging may lead to variations in mechanical properties between test specimens and the actual structure. Moreover, the experimental modal analysis was performed on a structure that had undergone operational use, potentially introducing micro-damage and structural defects that were not captured in the numerical model. The method currently assumes an idealized, defect-free material, which may lead to discrepancies when applied to real-world structures.

The methodology is particularly valuable for applications involving complex laminated composites, where traditional characterization methods may fall short. It enables comprehensive evaluation of material behaviour under operationally relevant dynamic conditions, supporting improved design validation, structural optimization, and virtual prototyping processes. Furthermore, because it relies primarily on modal data—which are relatively easy to acquire non-destructively—this approach is well-suited for integration into structural health monitoring frameworks and maintenance planning strategies.

Importantly, the proposed method is not limited to aerospace applications. It also shows strong potential for use in other sectors where composite materials are becoming increasingly prevalent, such as e-mobility, electric scooters, lightweight urban vehicles, automotive or wind farm blades. [48], [49], [50], [51] The growing reliance on advanced composites—driven by the demand for weight reduction, energy efficiency, and improved mechanical performance—creates a pressing need for reliable, non-destructive methods of structural assessment.

Further research should focus on accounting for structural aging effects, and exploring alternative optimization algorithms to enhance robustness. The optimization process will be expanded to include other metaheuristic techniques such as Particle Swarm Optimization (PSO) and Differential Evolution (DE), to evaluate their performance in terms of convergence rate, computational cost, and global search capability. These algorithms will be benchmarked against the current MOGA-based framework to assess sensitivity to initial conditions and parameter scaling.

Planned developments also include the implementation of more advanced surrogate models, such as Kriging and machine learning regressors, to reduce computational effort and improve model flexibility. Additionally, the methodology will be applied to a broader range of composite structures, including components made of natural fibre composites and thermoplastic laminates, to validate its versatility across different material systems and manufacturing methods. By addressing these factors, the proposed approach can serve as a powerful tool for improving the predictive capabilities of finite element models in aerospace and mechanical engineering applications.

References

1. M. Kucharski, M. Milewski, B. Dziewoński, K. Kaliszuk, T. Kisiel, and A. Kierzkowski, 'Flight Capability Analysis Among Different Latitudes for Solar Unmanned Aerial Vehicles', *Energies*, vol. 18, no. 6, Art. no. 6, Jan. 2025, doi: 10.3390/en18061331.
2. 'Home | Clean Aviation'. Accessed: May 20, 2025. [Online]. Available: https://www.clean-aviation.eu/
3. M. Karpenko and J. Nugaras, 'Vibration damping characteristics of the cork-based composite material in line to frequency analysis', *Journal of Theoretical and Applied Mechanics*, vol. 60, no. 4, pp. 593–602, Nov. 2022, doi: 10.15632/jtam-pl/152970.
4. A. Filippatos, D. Markatos, A. Theochari, and S. Pantelakis, 'Integrating Sustainability in Aircraft Component Design: Towards a Transition from Eco-Driven to Sustainability-Driven Design', *Aerospace*, vol. 12, no. 2, Art. no. 2, Feb. 2025, doi: 10.3390/aerospace12020140.
5. M. Karpenko *et al.*, 'Performance evaluation of extruded polystyrene foam for aerospace engineering applications using frequency analyses', *Int J Adv Manuf Technol*, vol. 126, no. 11, pp. 5515–5526, Jun. 2023, doi: 10.1007/s00170-023-11503-0.
6. P. Ragauskas and R. Belevičius, 'Identification of material properties of composite materials', *Aviation*, vol. 13, no. 4, Art. no. 4, Dec. 2009, doi: 10.3846/1648-7788.2009.13.109-115.
7. B. Rahmani, F. Mortazavi, I. Villemure, and M. Levesque, 'A new approach to inverse identification of mechanical properties of composite materials: Regularized model updating', *Composite Structures*, vol. 105, pp. 116–125, Nov. 2013, doi: 10.1016/j.compstruct.2013.04.025.
8. Y. L. Kang, X. H. Lin, and Q. H. Qin, 'Inverse/genetic method and its application in identification of mechanical parameters of interface in composite', *Composite Structures*, vol. 66, no. 1, pp. 449–458, Oct. 2004, doi: 10.1016/j.compstruct.2004.04.067.
9. B. Chen, Y. Zeng, H. Wang, and E. Li, 'Approximate Bayesian assisted inverse method for identification of parameters of variable stiffness composite laminates', *Composite Structures*, vol. 267, p. 113853, Jul. 2021, doi: 10.1016/j.compstruct.2021.113853.
10. D. Lecompte, A. Smits, H. Sol, J. Vantomme, and D. Van Hemelrijck, 'Mixed numerical–experimental technique for orthotropic parameter identification using biaxial tensile tests on cruciform specimens', *International Journal of Solids and Structures*, vol. 44, no. 5, pp. 1643–1656, Mar. 2007, doi: 10.1016/j.ijsolstr.2006.06.050.
11. M. G. D. Geers, R. de Borst, and T. Peijs, 'Mixed numerical-experimental identification of non-local characteristics of random-fibre-reinforced composites', *Composites Science and Technology*, vol. 59, no. 10, pp. 1569–1578, Aug. 1999, doi: 10.1016/S0266-3538(99)00017-2.
12. X. Liu, W. Sun, X. Yan, D. Du, H. Liu, and H. Li, 'Nonlinear vibration analysis of carbon fiber-reinforced composites with frequency-dependence and strain-dependence: Experimental and theoretical studies', *Thin-Walled Structures*, vol. 183, p. 110369, Feb. 2023, doi: 10.1016/j.tws.2022.110369.
13. M. Karpenko, P. Skačkauskas, and O. Prentkovskis, 'Methodology for the Composite Tire Numerical Simulation Based on the Frequency Response Analysis', *Eksploatacja i Niezawodność – Maintenance and Reliability*, vol. 25, no. 2, Apr. 2023, doi: 10.17531/ein/163289.
14. H. Lopes, S. P. Silva, and J. Machado, 'A simulation strategy to determine the mechanical behaviour of cork-rubber composite pads for vibration isolation', *Eksploatacja i Niezawodność – Maintenance and Reliability*, vol. 24, no. 1, pp. 80–88, Mar. 2022, doi: 10.17531/ein.2022.1.10.
15. J. Wittig, G. Tzortzinis, N. Modler, M. Lißner, and A. Filippatos, 'Vibration-based ice monitoring of composite blades using artificial neural networks under different icing conditions', *Cold Regions Science and Technology*, vol. 231, p. 104379, Mar. 2025, doi: 10.1016/j.coldregions.2024.104379.
16. T. H. Ooijevaar, R. Loendersloot, L. L. Warnet, A. de Boer, and R. Akkerman, 'Vibration based Structural Health Monitoring of a composite T-beam', *Composite Structures*, vol. 92, no. 9, pp. 2007–2015, Aug. 2010, doi: 10.1016/j.compstruct.2009.12.007.
17. Z. Liang, K. R. Ramakrishnan, C.-T. Ng, Z. Zhang, and J. Fu, 'Vibration-based prediction of residual fatigue life for composite laminates through frequency measurements', *Composite Structures*, vol. 329, p. 117771, Feb. 2024, doi: 10.1016/j.compstruct.2023.117771.
18. J. H. Tam, Z. C. Ong, C. L. Lau, Z. Ismail, B. C. Ang, and S. Y. Khoo, 'Identification of material properties of composite plates using Fourier-generated frequency response functions', *Mechanics of Advanced Materials and Structures*, vol. 26, no. 2, pp. 119–128, Jan. 2019, doi: 10.1080/15376494.2017.1365980.
19. M. F. Teixeira Silva *, L. M. S. Alves Borges, F. A. Rochinha, and L. A. V. De Carvalho, 'A genetic algorithm applied to composite elastic parameters identification', *Inverse Problems in Science and Engineering*, vol. 12, no. 1, pp. 17–28, Jan. 2004, doi:

10.1080/10682760310000979992.
20. S.-F. Hwang, J.-C. Wu, E. Barkanovs, and R. Belevicius, 'Elastic Constants of Composite Materials by an Inverse Determination Method Based on A Hybrid Genetic Algorithm', *Journal of Mechanics*, vol. 26, no. 3, pp. 345–353, Sep. 2010, doi: 10.1017/S1727719100003907.
21. A. L. Araújo, C. M. Mota Soares, M. J. Moreira de Freitas, P. Pedersen, and J. Herskovits, 'Combined numerical–experimental model for the identification of mechanical properties of laminated structures', *Composite Structures*, vol. 50, no. 4, pp. 363–372, Dec. 2000, doi: 10.1016/S0263-8223(00)00113-6.
22. P. Athi Sankar, R. Machavaram, and K. Shankar, 'System identification of a composite plate using hybrid response surface methodology and particle swarm optimization in time domain', *Measurement*, vol. 55, pp. 499–511, Sep. 2014, doi: 10.1016/j.measurement.2014.05.025.
23. Z. Ismail, H. Khov, and W. L. Li, 'Determination of material properties of orthotropic plates with general boundary conditions using Inverse method and Fourier series', *Measurement*, vol. 46, no. 3, pp. 1169–1177, Apr. 2013, doi: 10.1016/j.measurement.2012.11.005.
24. M. Jahanshahi, H. Shahbazi, and M. Heidari-Rarani, 'Locating delamination in a composite laminate using machine learning and recurrent deep neural networks based on vibration response', *Structures*, vol. 70, p. 107823, Dec. 2024, doi: 10.1016/j.istruc.2024.107823.
25. J. Wang, Z. Chang, G. Cao, and S.-K. Lai, 'Predicting delamination in composite laminates through semi-analytical dynamic analysis and vibration-based quantitative assessment', *Thin-Walled Structures*, vol. 204, p. 112346, Nov. 2024, doi: 10.1016/j.tws.2024.112346.
26. R. Gu, Y. Li, S. Zhang, J. Zhu, X. Pang, and Z. Liu, 'Structural vibration-based identification of delamination in CFRP cylinders using complex frequency domain correlation and CNN', *Composite Structures*, vol. 321, p. 117299, Oct. 2023, doi: 10.1016/j.compstruct.2023.117299.
27. S. Kilimtzidis *et al.*, 'Modeling, analysis and validation of the structural response of a large-scale composite wing by ground testing', *Composite Structures*, vol. 312, p. 116897, May 2023, doi: 10.1016/j.compstruct.2023.116897.
28. G. Dessena, D. I. Ignatyev, J. F. Whidborne, A. Pontillo, and L. Zanotti Fragonara, 'Ground Vibration Testing of a Flexible Wing: A Benchmark and Case Study', *Aerospace*, vol. 9, no. 8, Art. no. 8, Aug. 2022, doi: 10.3390/aerospace9080438.
29. V. Mugnaini, L. Zanotti Fragonara, and M. Civera, 'A machine learning approach for automatic operational modal analysis', *Mechanical Systems and Signal Processing*, vol. 170, p. 108813, May 2022, doi: 10.1016/j.ymssp.2022.108813.
30. P. Mohanty and D. J. Rixen, 'Identifying mode shapes and modal frequencies by operational modal analysis in the presence of harmonic excitation', *Experimental Mechanics*, vol. 45, no. 3, pp. 213–220, Jun. 2005, doi: 10.1007/BF02427944.
31. P. Avitabile, 'Experimental Modal Analysis (A Simple Non-Mathematical Presentation)'. University of Massachusetts Lowell. [Online]. Available: https://www.uml.edu/docs/s-v-jan2001_modal_analysis_tcm18-189939.pdf
32. J. Zhao, 'Basics of Modal Testing and Analysis'. Crystal Instruments Corporation, Jul. 2017.
33. A. Nettles, 'Basic Mechanics of Laminated composite plates', Oct. 1994.
34. V. Timhede, S. Timhede, S. Winyangkul, and S. Sleesongsom, 'Aircraft Wing Design Against Bird Strike Using Metaheuristics', *Aerospace*, vol. 12, no. 5, Art. no. 5, May 2025, doi: 10.3390/aerospace12050436.
35. J. Sauro and J. R. Lewis, 'Chapter 3 - How precise are our estimates? Confidence intervals', in *Quantifying the User Experience (Second Edition)*, J. Sauro and J. R. Lewis, Eds., Boston: Morgan Kaufmann, 2016, pp. 19–38. doi: 10.1016/B978-0-12-802308-2.00003-5.
36. L. M. S. Pereira, T. M. Milan, and D. R. Tapia-Blácido, 'Using Response Surface Methodology (RSM) to optimize 2G bioethanol production: A review', *Biomass and Bioenergy*, vol. 151, p. 106166, Aug. 2021, doi: 10.1016/j.biombioe.2021.106166.
37. C. Song and R. Kawai, 'Monte Carlo and variance reduction methods for structural reliability analysis: A comprehensive review', *Probabilistic Engineering Mechanics*, vol. 73, p. 103479, Jul. 2023, doi: 10.1016/j.probengmech.2023.103479.
38. ANSYS Inc., *DesignXplorer User's Guide*. 2024.
39. A. Kierzkowski, J. Wróbel, M. Milewski, and A. Filippatos, 'Sensitivity Analysis of Unmanned Aerial Vehicle Composite Wing Structural Model Regarding Material Properties and Laminate Configuration', *Drones*, vol. 9, no. 2, Art. no. 2, Feb. 2025, doi: 10.3390/drones9020099.
40. Department of Defense USA, 'Composite Materials Handbook. Volume 2. Polymer Matrix Composites Materials Properties'. Department of Defence USA, Jul. 17, 2002. [Online]. Available: https://www.waveequation.com/HDBK17-Volume2.pdf
41. 'Airex C70 Data Sheet'. Jul. 2011. [Online]. Available: https://www.3accorematerials.com/uploads/documents/TDS-AIREX-C70-E_1106.pdf

42. H. Karali, G. Inalhan, and A. Tsourdos, ‘Advanced UAV Design Optimization Through Deep Learning-Based Surrogate Models’, *Aerospace*, vol. 11, no. 8, Art. no. 8, Aug. 2024, doi: 10.3390/aerospace11080669.
43. X.-S. Yang, ‘Chapter 14 - Multi-Objective Optimization’, in *Nature-Inspired Optimization Algorithms*, X.-S. Yang, Ed., Oxford: Elsevier, 2014, pp. 197–211. doi: 10.1016/B978-0-12-416743-8.00014-2.
44. K. Deb, A. Pratap, S. Agarwal, and T. Meyarivan, ‘A fast and elitist multiobjective genetic algorithm: NSGA-II’, IEEE Transactions on Evolutionary Computation, vol. 6, no. 2, pp. 182–197, 2002, doi: 10.1109/4235.996017.
45. Standard Test Method for Tensile Properties of Polymer Matrix Composite Maerials, D3039.
46. Standard Test Method fro Compressive Properties of Polymer Matrix Composite Materials Using a Combined Loading Compression (CLC) Test Fixture, D6641.
47. ‘Standard Test Method for Shear Properties of Composite Materials by V-Notched Rail Shear Method’. Accessed: Oct. 23, 2024. [Online]. Available: https://www.astm.org/d7078_d7078m-05.html
48. M. Karpenko, O. Prentkovskis, and P. Skačkauskas, ‘Analysing the impact of electric kick-scooters on drivers: vibration and frequency transmission during the ride on different types of urban pavements’, *Eksploatacja i Niezawodność – Maintenance and Reliability*, vol. 27, no. 2, Jan. 2025, doi: 10.17531/ein/199893.
49. S. Zhang, H. Song, L. Xu, and K. Cai, ‘Application Research on the Lightweight Design and Optimization of Carbon Fiber Reinforced Polymers (CFRP) Floor for Automobile’, *Polymers*, vol. 14, no. 21, Art. no. 21, Jan. 2022, doi: 10.3390/polym14214768.
50. L. Yan and H. Xu, ‘Lightweight composite materials in automotive engineering: State-of-the-art and future trends’, Alexandria Engineering Journal, vol. 118, pp. 1–10, Apr. 2025, doi: 10.1016/j.aej.2024.12.002.
51. X. Cheng *et al.*, ‘A review of thermoplastic composites on wind turbine blades’, *Composites Part B: Engineering*, vol. 299, p. 112411, Jun. 2025, doi: 10.1016/j.compositesb.2025.112411.